Carbohydrate Polymers 106 (2014) 326–334

Contents lists available at ScienceDirect

Carbohydrate Polymers

journal homepage: www.elsevier.com/locate/carbpol

Bionanocomposites of regenerated cellulose/zeolite prepared using environmentally benign ionic liquid solvent

Mohammad Soheilmoghaddam[a], Mat Uzir Wahit[b,*], Wong Tuck Whye[a], Noel Ibrahim Akos[a], Raheleh Heidar Pour[a], Abdirahman Ali Yussuf[c]

[a] Department of Polymer Engineering, Faculty of Chemical Engineering, Universiti Teknologi Malaysia (UTM), Johor, Malaysia
[b] Center for Composites, Universiti Teknologi Malaysia (UTM), 81310 Skudai, Johor, Malaysia
[c] Petroleum Research and Studies Center, Kuwait Institute for Scientific Research, Safat, Kuwait

ARTICLE INFO

Article history:
Received 25 October 2013
Received in revised form 27 February 2014
Accepted 27 February 2014
Available online 11 March 2014

Keywords:
Regenerated cellulose
Zeolite
Bionanocomposite
Ionic liquid

ABSTRACT

Bionanocomposite films based on regenerated cellulose (RC) and incorporated with zeolite at different concentrations were fabricated by dissolving cellulose in 1-ethyl-3-methylimidazolium chloride (EMIMCl) ionic liquid using a simple green method. The interactions between the zeolite and the cellulose matrix were confirmed by Fourier transform infrared spectra. Mechanical properties of the nanocomposite films significantly improved as compared with the pure regenerated cellulose film, without the loss of extensibility. Zeolite incorporation enhanced the thermal stability and char yield of the nanocomposites. The scanning electron microscopy and transmission electron microscopy showed that zeolite was uniformly dispersed in the regenerated cellulose matrix. In vitro cytotoxicity test demonstrated that both RC and RC/zeolite nanocomposite films are cytocompatible. These results indicate that the prepared nanocomposites have potential applications in biodegradable packaging, membranes and biomedical areas.

1. Introduction

Cellulose, the most abundant and renewable resource in nature, is obtained from wood pulp and cotton and is considered a renewable chemical resource that can replace petroleum-based materials (Ma, Zhou, Li, Li, & Ou, 2011; Soheilmoghaddam, Wahit, & Ibrahim Akos, 2013; Soheilmoghaddam, Wahit, Mahmoudian, & Hanid, 2013). Cellulose a linear polysaccharide composed of β-1–4-linked D-glucopyranose repeating units, has drawn much attention due to its unique properties such as high mechanical strength, chemical stability, biodegradability and multitude of chemical derivations (Heinze & Liebert, 2001; Klemm, Heublein, Fink, & Bohn, 2005). However, on account of the extensive large network connecting hydrogen bonds and partially crystal structure, cellulose cannot be dissolved in water or most conventional organic solvents (Cai & Zhang, 2005; Song, Luo, Wang, Hao, & Gao, 2013). Therefore, several solvent systems such as *N*-methyl morpholine *N*-oxide (NMMO) (Fink, Weigel, Purz, & Ganster, 2001), lithium chloride/1,3-dimethyl-2-imidazolidinone (LiCl/DMI) (Takaragi, Minoda, Miyamoto, Liu, & Zhang, 1999), lithium chloride/*N*,*N*-dimethylacetamide (LiCl/DMAc) (McCormick & Callais, 1987) and phosphoric acid (Northolt et al., 2001) have been developed for the preparation of regenerated cellulose materials. Most of the systems developed thus far are still seen as unsuccessful in the eyes of industry and environmentalist because of their toxicity, difficult of solvent recovery and several adverse side reactions (Soheilmoghaddam, Wahit, & Ibrahim Akos, 2013; Soheilmoghaddam, Wahit, Mahmoudian, et al., 2013; Song et al., 2013).

Recently, a green solvent system known as ionic liquid (IL) has been gaining interest because of its potential to regenerate and chemically modify the cellulose (Swatloski, Spear, Holbrey, & Rogers, 2002). Ionic liquids are characterized by excellent dissolubility, low toxicity, thermal stability, near zero volatility and recyclability (Hameed, Guo, Tay, & Kazarian, 2011). The desirable properties of ILs can also be tailored since they offer great flexibility in the design of cationic and anionic structures and as such they are termed the "designers solvent" (Azubuike, Rodríguez, Okhamafe, & Rogers, 2012). Literature has shown a variety of ionic liquids (ILs) to be good cellulose and biomass non-derivating solvents (Casas et al., 2012; Fort et al., 2007; Jiang et al., 2011; Pu, Jiang, & Ragauskas, 2007). The most promising anions for cellulose dissolution are acetate and chloride, whereas different cations can be employed (Casas et al., 2012). The most common IL for cellulose dissolution

* Corresponding author. Tel.: +60 7 553 5909; fax: +60 7 553 6165.
E-mail address: mat.uzir@cheme.utm.my (M.U. Wahit).

http://dx.doi.org/10.1016/j.carbpol.2014.02.085
0144-8617/

is 1-ethyl-3-methylimidazolium chloride ([EMIM]$^+$[Cl]$^-$), producing a cellulose solution without derivation (Lan, Liu, Yue, Sun, & Kennedy, 2011; Swatloski et al., 2002).

Recently, organic–inorganic hybrid cellulose nanocomposites have attracted much attention due to their outstanding mechanical, optical, electrical and flame retardancy properties which are widely used in the fields of biomedicine, food packaging and water treatment (Han, Yan, Chen, Li, & Bangal, 2011). In the few past decades, polymer/zeolite nanocomposites have received a lot of attention as they perform better as compared to pure polymers. Zeolites are naturally occurring microporous framework silicates with a three-dimensional cage structure. They possess permanent negative charges in their structural framework which is balanced by exchangeable cations (Wang & Peng, 2010), thus they are widely used in adsorption, ion-exchange, catalysis and separation (Tosheva & Valtchev, 2005; Yu, Gong, Zeng, & Zhang, 2013). Zeolites have high mechanical strength, good thermal and chemical stability and nanocomposites reinforced with zeolites can be used over a wide range of operating conditions (Kittur, Kulkarni, Aralaguppi, & Kariduraganavar, 2005). Zeolites are also found to exhibit bioactivity and biocompatibility, thus they can be used as antibacterial materials, antitumor, anti-thrombotic agents, hemostatic, drug carriers and bone regenerants (Fatouros et al., 2011; McDonnell, Beving, Wang, Chen, & Yan, 2005; Wheatley et al., 2005). It is expected that the incorporation of zeolites into regenerated cellulose matrix may enhance the mechanical and thermal properties of the regenerated cellulose and also improve its biocompatibility.

In this work, regenerated cellulose/zeolite nanocomposite films were prepared via solution casting method. Ionic liquid was used as the key component medium for the dispersion of zeolite nanofiller and cellulose dissolution. The morphological, physical and mechanical properties of the bionanocomposite film were investigated in detail. Finally, cell viability assay was applied to understand the effect of zeolite on cellulose biocompatibility.

2. Experimental

2.1. Materials

Microcrystalline cellulose, a commercial reagent from Sigma with an average powder size of 50 μm, Avicel type with the degree of polymerization of 350 was used. The ionic liquid, 1-ethyl-3-methylimidazolium chloride (EMIMCl) with ≥95% purity. Zeolite (ZSM-5) with an average particle size of 300 nm and BET surface area of >362 m^2/g was purchased from advanced chemical supplier (ACS, USA).

2.2. Preparation of bionanocomposite films

The zeolite was dispersed in EMIMCL for 90 min using a sonicator (Model FB15053, 600 W maximum power, Fisher Scientific Co., Germany) before the addition of cellulose powder. In order to dissolve the cellulose in EMIMCL ionic liquid, the mixture was heated at 90 °C for 24 h with constant stirring. The ratio of EMIMCL/cellulose was 94/6 (wt.%). After degassing the solution in a vacuum oven, it was casted on a glass plate and immersed immediately in a distilled water bath at room temperature for 24 h to remove EMIMCL from the films. The obtained nanocomposite films were washed with water and dried in a vacuum oven at 40 °C for 2 h. All the dried films were stored in a moisture controlled desiccator for further testing. The RC/zeolite nanocomposites films prepared with different zeolite content (2, 4, 6 and 8 wt.% with respect to cellulose content) were coded as RC/Z2, RC/Z4, RC/Z6 and RC/Z8. The pure RC film was prepared with the same procedures as above without zeolite loading.

2.3. Characterization

2.3.1. UV–vis spectroscopy (UV–vis)

The optical transmittance (T_r) of the pure RC and RC/zeolite bionanocomposite films were measured with a UV–vis spectroscope (Shimadzu UV-3101PC, Japan) at wave lengths ranging from 200 to 800 nm.

2.3.2. Fourier transformed infrared spectroscopy (FTIR) measurement

The FTIR spectra were recorded on an attenuated total reflection Fourier transform infrared (ATR-FTIR) instrument (Nicolet Nexus 670, Thermo Fisher, USA) in the 157 range of 600–4000 cm^{-1} with a resolution of 4 cm^{-1}.

2.3.3. X-ray diffractometry (XRD)

X-ray diffraction (XRD) patterns were obtained using XRD diffractometer (Rigaku Miniflex II). Patterns with Cu Kα radiation (λ = 0.15406 nm) at 40 kV and 30 mA were recorded in the region of 2θ from 3 to 60.

2.3.4. Field emission scanning electron microscopy (FESEM)

The morphology of RC and RC/zeolite nanocomposite films was investigated by FESEM using a JEOL JSM-6701F SEM machine operating at an acceleration voltage of 5 kV. The micrographs were taken from the surface of cryofractured samples previously coated with gold. The elemental composition of RC and RC/zeolite nanocomposites was determined by energy dispersive X-ray (EDX) analysis (JEOL JSM-6701F SEM) coupled with FESEM.

2.3.5. Transmission electronic microscopy (TEM)

Ultrathin slices with the thickness of approximately 70–90 nm were obtained from nanocomposite film imbedded into an epoxy resin by ultra microtome (Power Tome XL) under cryogenic condition, and then placed into a carbon-coated copper grid. The dispersion state of zeolite within RC was investigated using Philips CM12 at an accelerating voltage of 200 kV.

2.3.6. Mechanical properties

Tensile properties were measured on an LRX Tensile Testing Machine (Lloyd, USA) according to ASTM D882-10 at a crosshead speed of 10 mm/min at room temperature. A gauge length of 30 mm was used. The specimens were cut into strips of 60 mm × 13 mm × 0.03 mm. The experiment was repeated five times and average values were taken.

2.3.7. Contact angle

Contact angles of water droplets with a volume of 2 μL on the films were measured at 23 °C and 50% RH using Face Water contact angle metre, Model CA-DT.A, Brand Kyowa.

2.3.8. Moisture uptake

Samples with dimensions (60 mm × 13 mm × 0.03 mm) were dried until constant weight in an oven at 85 °C for 24 h to remove moisture before the moisture absorption test. These samples were weighed immediately after removal from the oven. The samples were kept in a 75% constant relative humidity environment generated in a hermetic glass container with aqueous saturated NaCl solutions (ASTM E 104-02) at 25 °C. The moisture uptake (%*MU*) was calculated using Eq. (1):

$$\%MU = \frac{w_t - w_0}{w_0} \times 100 \quad (1)$$

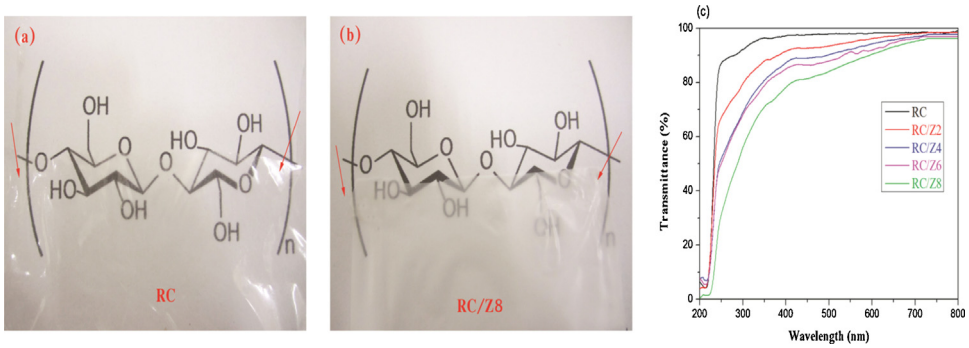

Fig. 1. The photographs of (a) RC, (b) RC/zeolite nanocomposite films with 8 wt.% zeolite content and (c) visible light transmittance of RC and their nanocomposite films.

where w_t and w_0 are each wet and initial dry film weight, respectively.

2.3.9. Water absorption

Water absorption test was conducted according to ASTM D570-98. Samples with dimensions of (76.2 mm × 25.4 mm × 0.03 mm) were dried to a constant weight under vacuum prior to immersion in distilled water at 25 °C for 2 and 24 h. Samples were removed from immersion and weight gains were recorded. The average value of five samples from every formulation was reported. The % weight gain was determined by Eq. (2):

$$\%\ \text{wieght gain} = \frac{w_w - w_d}{w_d} \times 100 \quad (2)$$

where w_d and w_w are the sample weights dry (before immersion) and wet (after immersion), respectively.

2.3.10. Thermal analysis

Thermal analysis of the RC/zeolite nanocomposite films was determined using Perkin Elmer TGA 7 (Perkin Elmer Instruments, USA). The temperature ranged from 30 to 800 °C with a heating rate of 10 °C min^{-1} under nitrogen.

2.3.11. Cytotoxicity analysis

Cell proliferation of the pure RC and RC/zeolite nanocomposite films were evaluated on human skin fibroblasts (HSF 1184) using dimethylthiazol diphenyl tetrazolium bromide (MTT) assay. All the films were sterilized by exposure to UV light for 6 h and followed by incubation in PBS solution for 24 h. Cells were seeded at a density of 2×10^5 cells/well onto the films in 96-well cell culture plates and incubated in a humidified chamber at 37 °C with 5% CO_2. After 24 h, 20 μL MTT solution (5 mg/ml) was added to each well. After incubation for 4 h at 37 °C, the medium was carefully removed and the intracellular formazan was dissolved by adding 200 μL dimethyl sulfoxide (DMSO) to each well. The absorbance was measured at 570 nm using a spectrophotometric microplate reader (Bio-Rad, Model 680, USA). The cells inoculated directly on tissue-culture polystyrene plate (TCPS) were regarded as a negative control. Tests were conducted in triplicate.

2.3.12. Statistical analysis

Multiple samples ($n = 3 - 6$) were collected in each experiment and expressed as mean ± standard deviation. Statistical comparisons were performed using one-way analysis of variance ANOVA with the post "Tukey's post hoc test" for multiple comparisons using SPSS software (SPSS, version 18). P values <0.05 were considered statistically significant.

3. Results and discussion

3.1. UV–vis spectroscopy (UV–vis)

Transmittance values (T_r) of films with the thickness of 30 ± 2.38 μm in the 200–800 nm range were measured (Fig. 1). The T_r values of film samples were compared at 550 nm since the human eye has the highest sensitivity at this wavelength (Liu, Zhang, Wu, Xiong, & Zhou, 2012). It is observed that transmittance of nanocomposite films remained above 87% (Fig. 1c). The optical transmittance of the pure RC film at 550 nm was 97.9%, and this value decreased to 87.4% for the nanocomposite with 8 wt.% zeolite. This was attributed to the uniform dispersion of zeolite nanofiller in the RC matrix as a result of the interfacial interactions between zeolite and RC. Similar observations have been reported for regenerated cellulose films reinforced by halloysite nano tube (HNT) and TiO_2 (Soheilmoghaddam & Wahit, 2013; Zhu et al., 2012).

3.2. Fourier transformed infrared spectroscopy (FTIR)

Chemical structure of zeolite, RC and nanocomposite films was analyzed using FTIR spectroscopy. Fig. 2 shows the main infrared spectral differences recorded as the characteristic peaks of zeolite, RC and RC/zeolite nanocomposite films. The zeolite spectrum shows a broad band in the range of 3300–3700 cm^{-1} which is attributed to the O—H stretching. The characteristic band at 1630 cm^{-1} is attributed to H—O—H bending (Christidis et al., 2003). A band in the range of 1230–980 cm^{-1} with a shoulder at 1210 cm^{-1} is assigned to the stretching vibrations Si(Al)—O. This band is sensitive to the structural content of Si and Al. A peak observed at 790 cm^{-1} is assigned to Si—O—Si band (Fig. 2a) (Castaldi et al., 2005).

The broad absorption band at 3000–3600 cm^{-1} in RC and RC/zeolite nanocomposite film is attributed to the O—H stretching in cellulose structure. The peak at 2923 cm^{-1} is assigned to C—H stretching vibration. The peaks at 1062 and 1164 cm^{-1} are attributed to alcoholic group C—OH. The high intensity peak at 1374 cm^{-1} is attributed to C—H/CH_2 bending vibration. The CH_2 symmetrical bending and C—O stretching vibration of C—O—C groups are located at 1430 and 894 cm^{-1}, respectively. The peak at 1635 cm^{-1} in the films is attributed to the absorbed water 'bending' vibration (Fig. 2a) (Han et al., 2011; Mahmoudian, Wahit, Imran, Ismail, & Balakrishnan, 2012; Mahmoudian, Wahit, Ismail, & Yussuf, 2012). The characteristic absorption peaks in the RC/zeolite curves are approximately similar to the pure cellulose curve. However, the position of the 3600–3000 cm^{-1} band intensities of RC nanocomposite films shift to lower wave numbers compared to that of RC film peak (Fig. 2b). In addition, the band at 1050–1090 cm^{-1} in the nanocomposite films are broadened because of the presence of SiO_2 in zeolite (encircled area in Fig. 2c), compared to cellulose (Dogan & Hilmioglu, 2009). The band at 790 cm^{-1} corresponding to the Si—O

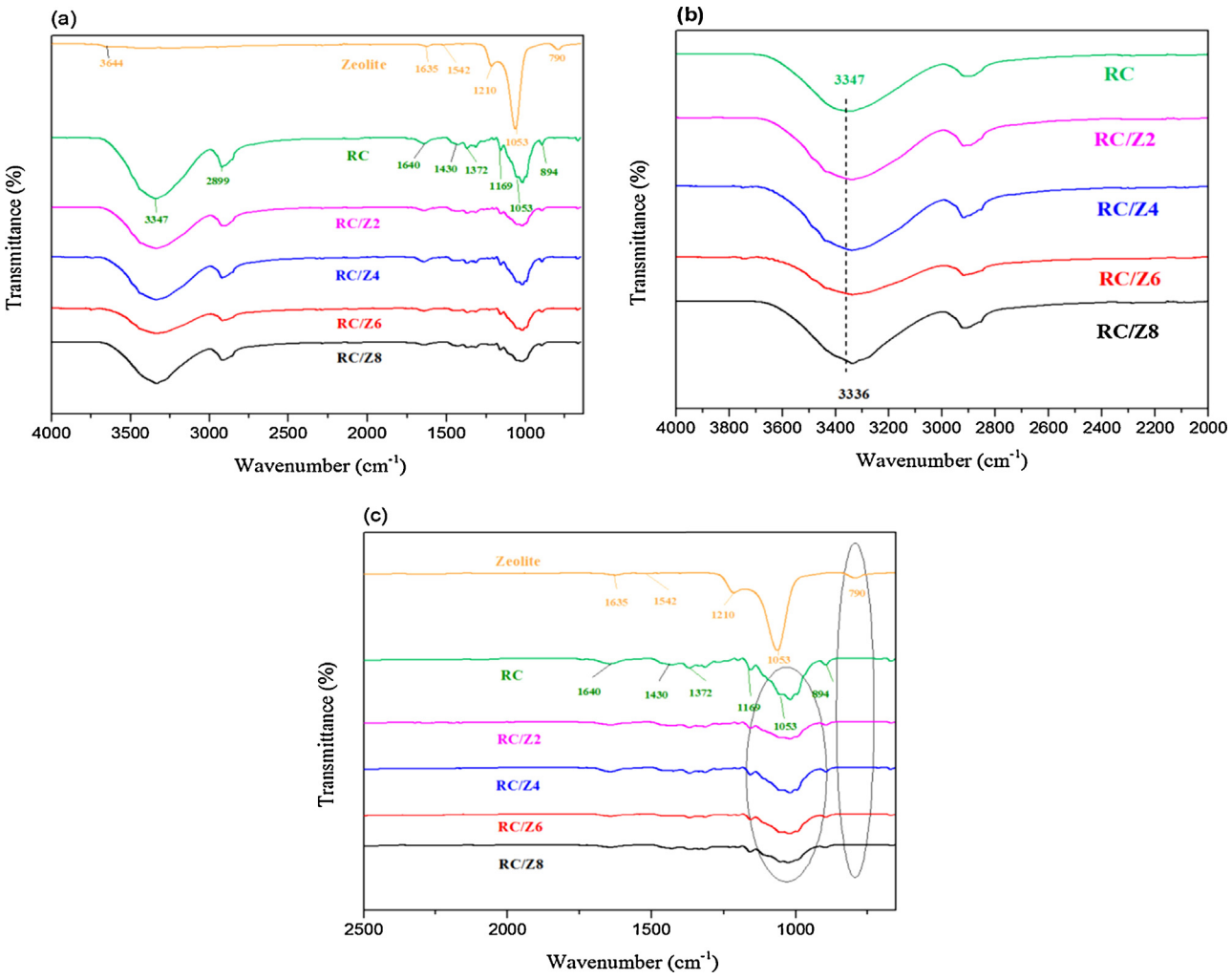

Fig. 2. FTIR spectra of (a) zeolite and RC nanocomposites, (b) RC and RC/zeolite nanocomposites at different zeolite contents and (c) zeolite, RC and RC/zeolite nanocomposites.

groups of zeolite disappeared in the nanocomposite films (Fig. 2c). These results reflect the formation of hydrogen bonds between the silanol groups (Si—O) of zeolite and the hydroxyls of RC. The results are consistent with the previous observation that hydrogen bonds are formed by the introduction of halloysite nanotubes into regenerated cellulose matrix (Hanid, Wahit, Guo, Mahmoodian, & Soheilmoghaddam, 2014; Soheilmoghaddam, Wahit, & Ibrahim Akos, 2013; Soheilmoghaddam, Wahit, Mahmoudian, et al., 2013).

3.3. X-ray diffractometry (XRD)

XRD patterns of the zeolite powder, RC and RC nanocomposite films with different loadings of zeolite are shown in Fig. 3. The regenerated cellulose films exhibit three characteristic peaks at around $2\theta = 12.1^\circ$ which correspond to $(1\,\bar{1}\,0)$ plane, whereas the sharper peaks at $2\theta = 20^\circ$ and $2\theta = 22^\circ$ correspond to $(1\,1\,0)$ and $(0\,2\,0)$ planes, respectively. These peaks are consistent with a transformation of cellulose I to cellulose II (Cai, Hou, & Yang, 2012; Han, Zhou, French, Han, & Wu, 2013; Soheilmoghaddam, Wahit, & Ibrahim Akos, 2013; Soheilmoghaddam, Wahit, Mahmoudian, et al., 2013). The diffraction angles of the nanocomposite films are similar to those of pure RC. The appearance of diffraction peaks for zeolite are expected at $2\theta = 7.9^\circ$, $2\theta = 8.8^\circ$, $2\theta = 23^\circ$, $2\theta = 24^\circ$, $2\theta = 29^\circ$ and $2\theta = 48^\circ$. Even though the peak at $2\theta = 24^\circ$ for zeolite still can be observed for RC/Z8 due to the fact that the peak was overlapped with the peak for RC. The other diffraction peaks corresponding to zeolite were not observed in the diffractograms of developed nanocomposite films (Fig. 3). This indicated that all the zeolite nanofillers were almost intercalated. The dispersion and intercalation of the zeolite nanofillers can be observed in the TEM images as discussed in following sections.

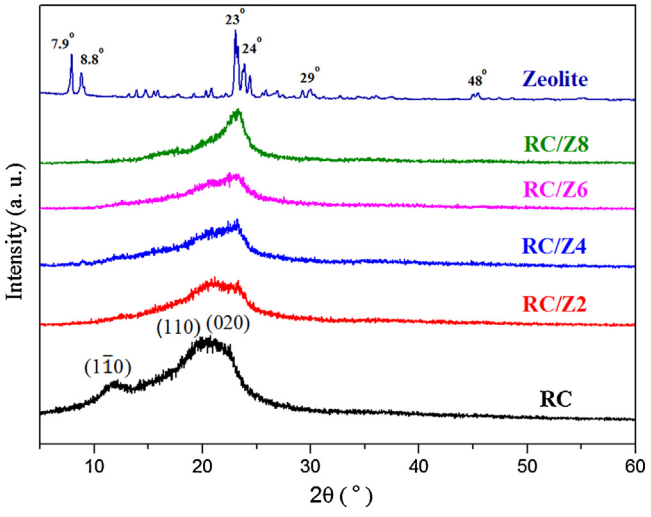

Fig. 3. XRD pattern of zeolite, RC and RC/zeolite nanocomposite films.

3.4. Morphology of the RC/zeolite nanocomposite films

The morphology of the RC and RC/ZC6 was investigated. The result revealed optimum mechanical properties for the nanocomposites with 6 wt.% zeolites. In view of the above, the composite with 6 wt.% was selected for SEM and TEM.

FESEM images of the top surface and cross sectional views of the pure RC and RC/zeolite nanocomposite film with 6 wt.% zeolite content. The top surface of the RC film appears smooth and uniform (Fig. 4a) while an increase in surface roughness was detected with the presence of zeolite nanofillers (Fig. 4b). Fig. 4c shows the nonporous structure of dense RC film. The FESEM images of the nanocomposites show that zeolite is uniformly dispersed in the RC matrix (Fig. 4d). In addition, the photographs clearly show that the zeolite nanofillers were embedded in the RC matrix and the RC appeared to cover the surface of zeolite (Fig. 4f–h). This is attributed to the interfacial interaction between the zeolites and RC. Fig. 4i and j shows the EDX elemental analysis spectra of RC and RC/zeolite nanocomposite films. Elemental analysis of RC and its nanocomposite showed elemental carbon (C), oxygen (O) and platinum (Pt) signals. Elemental C and O signals correspond to chemical formulation of cellulose while Pt corresponded to the coating of the films that was applied before FESEM and EDX testing (Fig. 4i). The absence of elemental nitrogen (N) in the composites indicates the complete removal of the ionic liquid from the films. Elemental N signal is a signature peak for the ionic liquids (Barroso, Temtem, Hussain, Aguiar-Ricardo, & Roque, 2010; Li, Zhang, & Xu, 2012). The elemental signals which correspond to the chemical formulation of zeolite were clearly observed in the nanocomposite film (Fig. 4j).

TEM images showed that the zeolite was well-dispersed in RC/Z6 nanocomposite film and the average particle size was <250 nm (Fig. 5). This homogenous dispersion of the zeolite in RC matrix is consistent with the FESEM results (Fig. 4).

3.5. Mechanical strength

The mechanical properties of the pure RC and the RC/zeolite nanocomposite films were investigated to determine the effects of zeolite incorporation on mechanical strength of RC. The results for tensile strength and Yong's modulus of the RC and its nanocomposite films are shown in Table 1. The results show that the tensile strength and Young's modulus significantly increased ($P < 0.05$ one-way ANOVA Tukey's post hoc test) as compared to the pure RC film. The tensile strength of pure RC film increased from 35.30 ± 1.12 MPa for pure RC film to 81.10 ± 0.95 MPa at 6 wt.% zeolite addition. This is a 130% improvement in tensile strength at 6 wt.% zeolite content. Similar improvement in the tensile properties of RC/HNT nanocomposites have been reported (Hanid et al., 2014). Above 6 wt.% zeolite content, tensile strength reduced slightly due to the fact that additional filler loading is attributed to the agglomeration of the zeolite nanofillers. The filler loading increment enhanced the filler attraction force within the zeolites, thus decreasing the surface area for the stress transfer (Vadukumpully, Paul, Mahanta, & Valiyaveettil, 2011). The increase in zeolite content also led to a significant increase in Young's modulus, from 1.8 ± 0.93 GPa for pure RC to 4.6 ± 0.55 GPa for RC/zeolite nanocomposite at 8 wt.% zeolite content. This improvement in the mechanical properties of the RC/zeolite nanocomposite films was attributed to the strong interaction between the zeolite and the hydroxyl groups of RC matrix. This improvement in the mechanical properties may also be ascribed to the good dispersion of zeolite in the intercalated form which provides more interfacial regions for more efficient stress transfer to the zeolite particles (Mahmoudian, Wahit, Imran, et al., 2012; Mahmoudian, Wahit, Ismail, et al., 2012).

Table 1
The mechanical, thermal, contact angle, moisture uptake and water absorption properties of RC and RC/zeolite nanocomposite films.

Samples	Young's modulus (GPa)	Tensile strength (MPa)	Elongation at break (%)	T_{20} (°C)	T_{50} (°C)	DTG (°C)	Residue (%) at 750 (°C)	Contact angle (°)				Moisture uptake (%)	Water absorption (%)	
								1 (s)	5 (s)	10 (s)	15 (s)		2 (h)	24 (h)
RC	1.8 ± 0.93^{a}	35.30 ± 1.12^{d}	5.26 ± 0.72^{i}	320	361	351	0.3	27.5 ± 1.8^{k}	27 ± 2.4^{n}	26.5 ± 1.6^{q}	26.5 ± 2.4^{s}	14.7 ± 1.8^{b}	105 ± 1.5^{c}	108.6 ± 1.7^{f}
RC/Z2	$3.1 \pm 0.95^{a,b}$	64.20 ± 0.70^{e}	6.90 ± 0.56^{j}	332	370	362	9.9	30 ± 2.2^{k}	28 ± 2.2^{n}	27.5 ± 2.1^{q}	27.5 ± 2.1^{s}	14.5 ± 2.1^{a}	97.2 ± 1.3^{b}	104.1 ± 1.2^{e}
RC/Z4	$3.3 \pm 0.63^{a,b}$	69.80 ± 0.53^{f}	6.95 ± 0.98^{j}	337	376	370	15.7	33 ± 2.3^{l}	30.5 ± 1.8^{o}	29.2 ± 2.5^{q}	29.2 ± 1.7^{s}	13.6 ± 2.2^{a}	95.8 ± 1.5^{b}	102.3 ± 1.5^{e}
RC/Z6	$4.2 \pm 0.75^{b,c}$	81.10 ± 0.95^{h}	7.58 ± 1.00^{j}	346	406	375	21.9	48.5 ± 1.9^{m}	47 ± 2.6^{p}	46 ± 2.2^{r}	46 ± 2.2^{t}	11.9 ± 1.8^{a}	91.2 ± 1.0^{a}	94.4 ± 1.3^{d}
RC/Z8	4.6 ± 0.55^{c}	71.80 ± 1.33^{g}	7.54 ± 1.20^{j}	346	393	375	18.9	46 ± 2.4^{m}	44 ± 2.2^{p}	43.5 ± 1.9^{r}	43.5 ± 2.4^{t}	12 ± 1.2^{a}	93.4 ± 1.1^{b}	92.1 ± 1.2^{d}

Value for each film is the mean ± standard deviation. Values with different superscript letters are significantly different ($P < 0.05$) according to the *T* Tukey's post hoc tests.

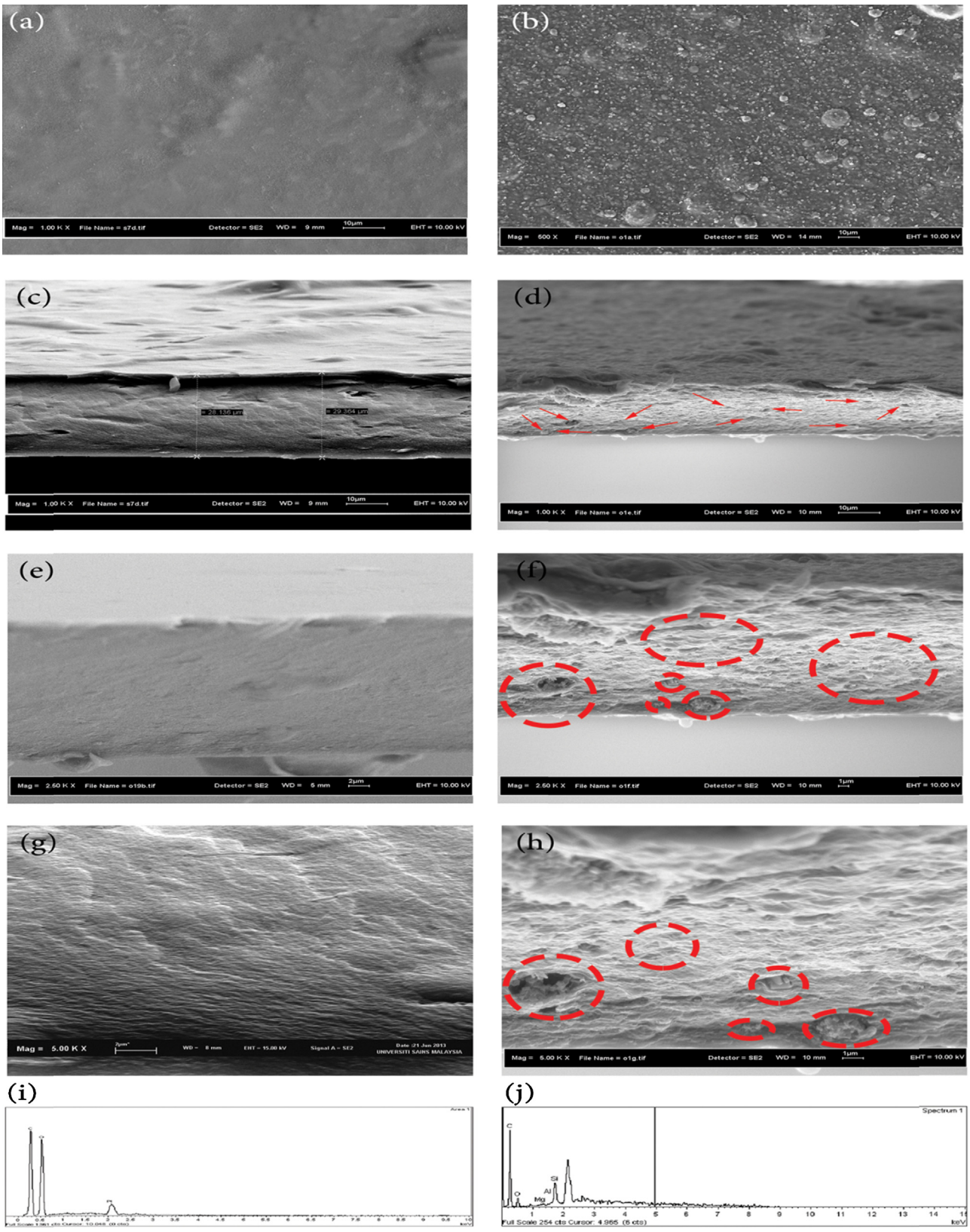

Fig. 4. FESEM images of top surface of (a) RC, (b) RC/Z6. Cross sectional of (c)–(e)–(g) RC, (d)–(f)–(b) RC/Z6. EDX spectra (i) RC, and (j) RC/Z6.

The elongation at break of RC/zeolite nanocomposites at (0–8 wt.%) zeolite loading is shown in Table 1. It is obvious that the elongation at break of the nanocomposites increases as zeolite loading increases from 0 to 6 wt.% zeolite content. The elongation at break of the RC/zeolite nanocomposite films with 6 wt.% was 43% higher than pure RC film, after which it was nearly constant. It is believed that the improvement in stiffness as well as ductility in the nanocomposites is due to the strong interaction between the

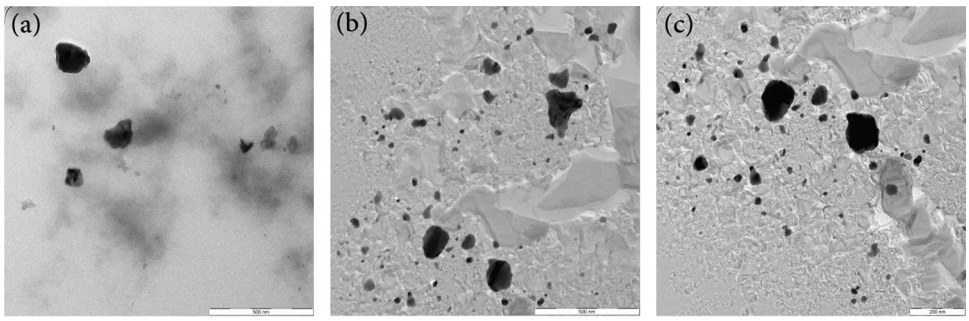

Fig. 5. TEM pictures of RC/Z6 nanocomposite film at (a) and (b) 20K, and (c) 25K.

homogeneous dispersed zeolite and RC matrix. The same trend has been reported when HNT and grapheme oxide was incorporated into RC matrix (Han et al., 2011; Soheilmoghaddam & Wahit, 2013).

3.6. Hydrophilicity of cellulose/zeolite nanocomposite films

The contact angle (CA) of water droplet was used to estimate the degree of hydrophilicity or hydrophobicity of the film surface. The results of water contact angle for the RC and RC/zeolite nanocomposite films over time are shown in Table 1. The results reveal that the use of zeolite led to a reduction in hydrophilicity of the nanocomposite films compared to the pure RC film. The contact angle of pure RC film with water was found to be $27.5 \pm 1.8^{\circ}$ after 1 s and remained almost unchanged over time, which implies that the films are intrinsically hydrophilic. In contrast, the contact angle value for RC nanocomposite film with 6 wt.% zeolite content was $48.5 \pm 1.9^{\circ}$. The reduction in hydrophilicity of the nanocomposites is attributed to the strong interaction between the RC and lower hydrophilic zeolite nanoparticles, which are equally dispersed in the matrix. Other researchers have also reported similar results for RC reinforced with MMT (Mahmoudian, Wahit, Imran, et al., 2012; Mahmoudian, Wahit, Ismail, et al., 2012).

Moisture content of the RC and RC/zeolite nanocomposite films was determined at RH = 75% and 25 °C temperature. The results of moisture absorption (%) for the nanocomposite films as a function of zeolite content are shown in Table 1. The MA% of the nanocomposite decreased from $14.7 \pm 1.8\%$ to $12 \pm 1.2\%$ as the zeolite content increased from 0 wt.% to 8 wt.%. In another experiment, RC and its nanocomposite films were immersed in water for 2 h and 24 h to measure water uptake (Table 1). It was observed that the addition of zeolite improved the water resistance of RC. Water absorption of the nanocomposite films decreased from $108.6 \pm 1.7\%$ to $92.1 \pm 1.2\%$ as zeolite content increased from 0 to 8 wt.% after 24 h.

These decreases in moisture content and water uptake for the nanocomposite films is attributed to the potential of hydrogen bond formation between zeolite and RC which will result in the formation of a strong structure which in turn reduces the diffusion of water molecules in the material. Other researchers have also reported similar results for RC nanocomposite films based on MMT and HNT (Hanid et al., 2014; Mahmoudian, Wahit, Imran, et al., 2012; Mahmoudian, Wahit, Ismail, et al., 2012; Soheilmoghaddam & Wahit, 2013).

3.7. Thermal stability analysis

Fig. 6 shows thermogravimetric analysis (TGA) and differential thermogravimetry (DTG) curves of zeolite and the nanocomposite films. The 20 wt.% weight loss temperature (T_{20}) and 50 wt.% weight loss temperature (T_{50}) of samples are shown in Table 1. As shown, the zeolite powder decomposed around 10 wt.% in 450–600 °C range. The zeolite loading had a significant effect on the thermal stability of RC nanocomposites. The TGA image revealed that as low as 2 wt.% of zeolite (RC/Z2), was able to improve the RC nanocomposite films thermal behaviour. As the zeolite loadings increase, the thermal behaviour was shifted towards higher temperature compared to neat RC. For the pure cellulose film, T_{20} = 320 °C and T_{50} = 361 °C, while for the RC nanocomposite film with 6 wt.% zeolite content, T_{20} = 246 °C and T_{50} = 406 °C. It can also be seen that the char yields for the nanocomposite films increased with zeolite incorporation into the nanocomposite films. The char yield of RC

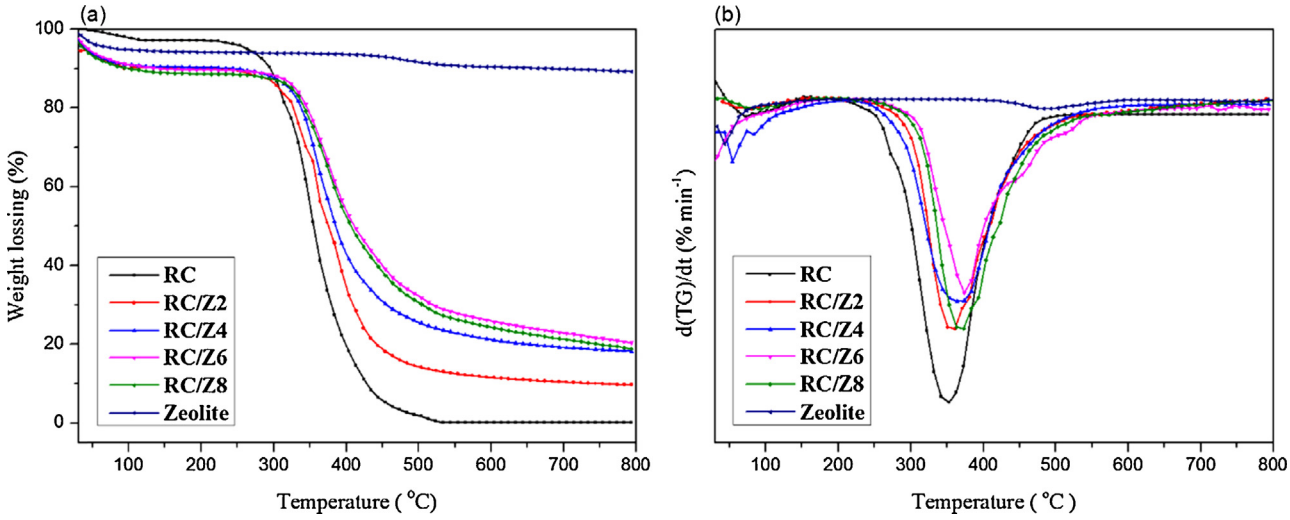

Fig. 6. The (a) TGA, (b) DTG curves of zeolite, RC and its nanocomposite films.

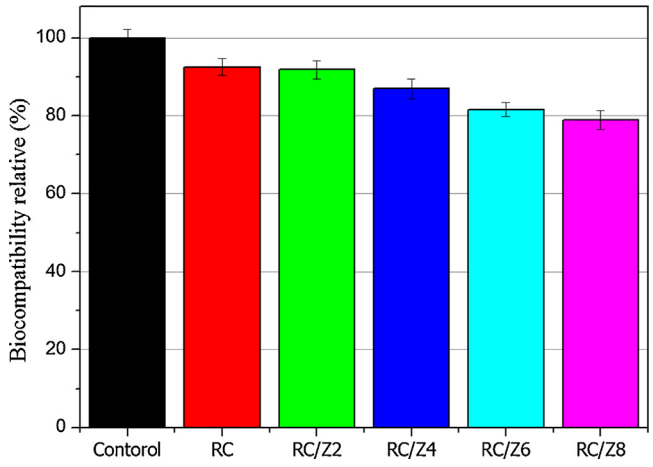

Fig. 7. Cytotoxicity test of RC and RC/zeolite nanocomposite films on human skin fibroblasts (HSF 1184) cell (mean values ± s.e.; $n = 3$).

was 0.3% at 750 °C, whereas at the same temperature it increased to 21.9% for the nanocomposites with 6 wt.% zeolite content. However, the massive residue increase is not proportional to the zeolite content. The increase in thermal stability and char yields of the nanocomposites is attributed to the thermal insulation effect of the well dispersed zeolite in RC matrix and also the entrapment of volatile RC products inside the microporous zeolite structure. Previous studies on chitosan/zeolite nanocomposites also reported the higher thermal stability of the nanocomposites due to interaction between the zeolite and the chitosan (Yu et al., 2013).

3.8. In vitro cytotoxicity test

The ability of the RC and RC/zeolite nanocomposites to support cell viability and proliferation on human skin fibroblasts (HSF 1184) showed that the evaluated samples were biocompatible according to the standard of ISO 10993-5 (Fig. 7). As shown in Fig. 7, no significant reduction in cell viability was observed for the RC and RC/zeolite nano composites as the zeolite content increased up to 6 wt. % ($P > 0.05$ one way ANOVA Tukey's post hoc test.). Previous reports have also shown that zeolite based polymer nano composites are noncytotoxic to various cells (Ninan et al., 2014; Seifu, Isimjan, & Mequanint, 2011). The percentage cell viability for RC and RC/Z6 was 92.48 ± 2.21% and 81.61 ± l.42%, respectively. The lowest percentage of 78.88 ± 2.58% for cell viability was observed for RC/Z8. The reduction in the cell viability for the composites with 8 wt.% zeolite is attributed to the death of cells which is caused by the agglomeration of the nanofillers. This implies that high quantity of clay particles blocked most of the channels on the cell membrane thus leading to the death of the cells. Other researchers have reported similar findings (Liu, Wu, Jiao, Xiong, & Zhou, 2013; Salcedo et al., 2012). Cytotoxicity tests using cell cultures have been accepted as the first step in identifying active compounds and for biosafety testing (Costa-Júnior, Barbosa-Stancioli, Mansur, Vasconcelos, & Mansur, 2009; Liu et al., 2012; Mansur, de S. Costa, Mansur, & Barbosa-Stancioli, 2009). Consequently, it can be inferred from the MTT results that all the nanocomposite films produced in the present research have the potential to be tested in vivo assays.

4. Conclusions

Zeolite nanoparticles were successfully incorporated into cellulose matrix using EMIMCl solvent as a simple and low cost method. The results suggested strong interaction between the silanol groups of zeolite and the hydroxyls of RC due to the formation of strong hydrogen bonds. The zeolite nanoparticles were uniformly dispersed and embedded in the inorganic–organic films. The thermal stability and mechanical properties of RC are significantly improved upon the addition of zeolite without the loss of extensibility. The water contact angle and moisture absorption test showed more hydrophobicity of the nanocomposites when compared with pure RC. The cytotoxicity results on human skin fibroblasts (HSF 1184) cell revealed that the nanocomposite films were not toxic and biocompatible, thus showing potential application in biomaterials.

Acknowledgements

The authors wish to acknowledge the Fundamental Research Grant Scheme (FRGS) Vote No: GUP00H27 by Universiti Teknologi Malaysia from the Ministry of Science, Technology and Innovation (MOSTI).

References

Azubuike, C., Rodríguez, H., Okhamafe, A., & Rogers, R. (2012). Physicochemical properties of maize cob cellulose powders reconstituted from ionic liquid solution. *Cellulose*, *19*(2), 425–433.

Barroso, T., Temtem, M., Hussain, A., Aguiar-Ricardo, A., & Roque, A. C. A. (2010). Preparation and characterization of a cellulose affinity membrane for human immunoglobulin G (IgG) purification. *Journal of Membrane Science*, *348*(1–2), 224–230.

Cai, J., & Zhang, L. (2005). Unique gelation behavior of cellulose in NaOH/urea aqueous solution. *Biomacromolecules*, *7*(1), 183–189.

Cai, Z., Hou, C., & Yang, G. (2012). Characteristics and bending performance of electroactive polymer blend made with cellulose and poly(3-hydroxybutyrate). *Carbohydrate Polymers*, *87*(1), 650–657.

Casas, A., Palomar, J., Alonso, M. V., Oliet, M., Omar, S., & Rodriguez, F. (2012). Comparison of lignin and cellulose solubilities in ionic liquids by COSMO-RS analysis and experimental validation. *Industrial Crops and Products*, *37*(1), 155–163.

Castaldi, P., Santona, L., Cozza, C., Giuliano, V., Abbruzzese, C., Nastro, V., et al. (2005). Thermal and spectroscopic studies of zeolites exchanged with metal cations. *Journal of Molecular Structure*, *734*(1–3), 99–105.

Christidis, G. E., Moraetis, D., Keheyan, E., Akhalbedashvili, L., Kekelidze, N., Gevorkyan, R., et al. (2003). Chemical and thermal modification of natural HEU-type zeolitic materials from Armenia, Georgia and Greece. *Applied Clay Science*, *24*(1–2), 79–91.

Costa-Júnior, E. S., Barbosa-Stancioli, E. F., Mansur, A. A. P., Vasconcelos, W. L., & Mansur, H. S. (2009). Preparation and characterization of chitosan/poly(vinyl alcohol) chemically crosslinked blends for biomedical applications. *Carbohydrate Polymers*, *76*(3), 472–481.

Dogan, H., & Hilmioglu, N. D. (2009). Dissolution of cellulose with NMMO by microwave heating. *Carbohydrate Polymers*, *75*(1), 90–94.

Fatouros, D. G., Douroumis, D., Nikolakis, V., Ntais, S., Moschovi, A. M., Trivedi, V., et al. (2011). In vitro and in silico investigations of drug delivery via zeolite BEA. *Journal of Materials Chemistry*, *21*(21), 7789–7794.

Fink, H. P., Weigel, P., Purz, H. J., & Ganster, J. (2001). Structure formation of regenerated cellulose materials from NMMO-solutions. *Progress in Polymer Science*, *26*(9), 1473–1524.

Fort, D. A., Remsing, R. C., Swatloski, R. P., Moyna, P., Moyna, G., & Rogers, R. D. (2007). Can ionic liquids dissolve wood? Processing and analysis of lignocellulosic materials with 1-n-butyl-3-methylimidazolium chloride. *Green Chemistry*, *9*(1), 63–69.

Hameed, N., Guo, Q., Tay, F. H., & Kazarian, S. G. (2011). Blends of cellulose and poly(3-hydroxybutyrate-co-3-hydroxyvalerate) prepared from the ionic liquid 1-butyl-3-methylimidazolium chloride. *Carbohydrate Polymers*, *86*(1), 94–104.

Han, D., Yan, L., Chen, W., Li, W., & Bangal, P. R. (2011). Cellulose/graphite oxide composite films with improved mechanical properties over a wide range of temperature. *Carbohydrate Polymers*, *83*(2), 966–972.

Han, J., Zhou, C., French, A. D., Han, G., & Wu, Q. (2013). Characterization of cellulose II nanoparticles regenerated from 1-butyl-3-methylimidazolium chloride. *Carbohydrate Polymers*, *94*(2), 773–781.

Hanid, N. A., Wahit, M. U., Guo, Q., Mahmoodian, S., & Soheilmoghaddam, M. (2014). Development of regenerated cellulose/halloysites nanocomposites via ionic liquids. *Carbohydrate Polymers*, *99*, 91–97.

Heinze, T., & Liebert, T. (2001). Unconventional methods in cellulose functionalization. *Progress in Polymer Science*, *26*(9), 1689–1762.

Jiang, M., Zhao, M., Zhou, Z., Huang, T., Chen, X., & Wang, Y. (2011). Isolation of cellulose with ionic liquid from steam exploded rice straw. *Industrial Crops and Products*, *33*(3), 734–738.

Kittur, A. A., Kulkarni, S. S., Aralaguppi, M. I., & Karidurganavar, M. Y. (2005). Preparation and characterization of novel pervaporation membranes for the separation of water–isopropanol mixtures using chitosan and NaY zeolite. *Journal of Membrane Science*, *247*(1–2), 75–86.

Klemm, D., Heublein, B., Fink, H.-P., & Bohn, A. (2005). Cellulose: Fascinating biopolymer and sustainable raw material. *Angewandte Chemie International Edition*, *44*(22), 3358–3393.

Lan, W., Liu, C.-F., Yue, F.-X., Sun, R.-C., & Kennedy, J. F. (2011). Ultrasound-assisted dissolution of cellulose in ionic liquid. *Carbohydrate Polymers*, *86*(2), 672–677.

Li, R., Zhang, L., & Xu, M. (2012). Novel regenerated cellulose films prepared by coagulating with water: Structure and properties. *Carbohydrate Polymers*, *87*(1), 95–100.

Liu, M., Wu, C., Jiao, Y., Xiong, S., & Zhou, C. (2013). Chitosan–halloysite nanotubes nanocomposite scaffolds for tissue engineering. *Journal of Materials Chemistry B*, *1*(15), 2078–2089.

Liu, M., Zhang, Y., Wu, C., Xiong, S., & Zhou, C. (2012). Chitosan/halloysite nanotubes bionanocomposites: Structure, mechanical properties and biocompatibility. *International Journal of Biological Macromolecules*, *51*(4), 566–575.

Ma, H., Zhou, B., Li, H.-S., Li, Y.-Q., & Ou, S.-Y. (2011). Green composite films composed of nanocrystalline cellulose and a cellulose matrix regenerated from functionalized ionic liquid solution. *Carbohydrate Polymers*, *84*(1), 383–389.

Mahmoudian, S., Wahit, M. U., Imran, M., Ismail, A. F., & Balakrishnan, H. (2012). A facile approach to prepare regenerated cellulose/graphene nanoplatelets nanocomposite using room-temperature ionic liquid. *Journal of Nanoscience and Nanotechnology*, *12*(7), 5233–5239.

Mahmoudian, S., Wahit, M. U., Ismail, A. F., & Yussuf, A. A. (2012). Preparation of regenerated cellulose/montmorillonite nanocomposite films via ionic liquids. *Carbohydrate Polymers*, *88*(4), 1251–1257.

Mansur, H. S., de S. Costa, E., Jr., Mansur, A. A. P., & Barbosa-Stancioli, E. F. (2009). Cytocompatibility evaluation in cell-culture systems of chemically crosslinked chitosan/PVA hydrogels. *Materials Science and Engineering: C*, *29*(5), 1574–1583.

McCormick, C. L., & Callais, P. A. (1987). Derivatization of cellulose in lithium chloride and N-N-dimethylacetamide solutions. *Polymer*, *28*(13), 2317–2323.

McDonnell, A. M. P., Beving, D., Wang, A., Chen, W., & Yan, Y. (2005). Hydrophilic and antimicrobial zeolite coatings for gravity-independent water separation. *Advanced Functional Materials*, *15*(2), 336–340.

Ninan, N., Muthiah, M., Bt Yahaya, N. A., Park, I.-K., Elain, A., Wong, T. W., et al. (2014). Antibacterial and wound healing analysis of gelatin/zeolite scaffolds. *Colloids and Surfaces B: Biointerfaces*, *115*, 244–252.

Northolt, M. G., Boerstoel, H., Maatman, H., Huisman, R., Veurink, J., & Elzerman, H. (2001). The structure and properties of cellulose fibres spun from an anisotropic phosphoric acid solution. *Polymer*, *42*(19), 8249–8264.

Pu, Y., Jiang, N., & Ragauskas, A. J. (2007). Ionic liquid as a green solvent for lignin. *Journal of Wood Chemistry and Technology*, *27*(1), 23–33.

Salcedo, I., Aguzzi, C., Sandri, G., Bonferoni, M. C., Mori, M., Cerezo, P., et al. (2012). In vitro biocompatibility and mucoadhesion of montmorillonite chitosan nanocomposite: A new drug delivery. *Applied Clay Science*, *55*(0), 131–137.

Seifu, D. G., Isimjan, T. T., & Mequanint, K. (2011). Tissue engineering scaffolds containing embedded fluorinated-zeolite oxygen vectors. *Acta Biomaterialia*, *7*(10), 3670–3678.

Soheilmoghaddam, M., Wahit, M. U., & Ibrahim Akos, N. (2013). Regenerated cellulose/epoxidized natural rubber blend film. *Materials Letters*, *111*, 221–224.

Soheilmoghaddam, M., & Wahit, M. U. (2013). Development of regenerated cellulose/halloysite nanotube bionanocomposite films with ionic liquid. *International Journal of Biological Macromolecules*, *58*, 133–139.

Soheilmoghaddam, M., Wahit, M. U., Mahmoudian, S., & Hanid, N. A. (2013). Regenerated cellulose/halloysite nanotube nanocomposite films prepared with an ionic liquid. *Materials Chemistry and Physics*, *141*(2–3), 936–943.

Song, H.-Z., Luo, Z.-Q., Wang, C.-Z., Hao, X.-F., & Gao, J.-G. (2013). Preparation and characterization of bionanocomposite fiber based on cellulose and nano-SiO_2 using ionic liquid. *Carbohydrate Polymers*, *98*(1), 161–167.

Swatloski, R. P., Spear, S. K., Holbrey, J. D., & Rogers, R. D. (2002). Dissolution of cellulose with ionic liquids. *Journal of the American Chemical Society*, *124*(18), 4974–4975.

Takaragi, A., Minoda, M., Miyamoto, T., Liu, H., & Zhang, L. (1999). Reaction characteristics of cellulose in the LiCl/1,3-dimethyl-2-midazolidinone solvent system. *Cellulose*, *6*(2), 93–102.

Tosheva, L., & Valtchev, V. P. (2005). Nanozeolites: Synthesis, crystallization mechanism, and applications. *Chemistry of Materials*, *17*(10), 2494–2513.

Vadukumpully, S., Paul, J., Mahanta, N., & Valiyaveettil, S. (2011). Flexible conductive graphene/poly(vinyl chloride) composite thin films with high mechanical strength and thermal stability. *Carbon*, *49*(1), 198–205.

Wang, S., & Peng, Y. (2010). Natural zeolites as effective adsorbents in water and wastewater treatment. *Chemical Engineering Journal*, *156*(1), 11–24.

Wheatley, P. S., Butler, A. R., Crane, M. S., Fox, S., Xiao, B., Rossi, A. G., et al. (2005). NO-releasing zeolites and their antithrombotic properties. *Journal of the American Chemical Society*, *128*(2), 502–509.

Yu, L., Gong, J., Zeng, C., & Zhang, L. (2013). Preparation of zeolite-A/chitosan hybrid composites and their bioactivities and antimicrobial activities. *Materials Science and Engineering: C*, *33*(7), 3652–3660.

Zhu, T., Lin, Y., Luo, Y., Hu, X., Lin, W., Yu, P., et al. (2012). Preparation and characterization of TiO_2-regenerated cellulose inorganic–polymer hybrid membranes for dehydration of caprolactam. *Carbohydrate Polymers*, *87*(1), 901–909.